Fizika Nizkikh Temperatur, 2009, v. 35, No. 4, p. 413–422

Pathways to metallic hydrogen

Isaac F. Silvera and Shanti Deemyad

Harvard University, Cambridge, MA 02138, USA
E-mail: silvera@physics.physics.edu

Received December 12, 2008

The traditional pathway that researchers have used in the goal of producing atomic metallic hydrogen is to compress samples with megabar pressures at low temperature. A number of phases have been observed in solid hydrogen and its isotopes, but all are in the insulating phase. The results of experiment and theory for this pathway are reviewed. In recent years a new pathway has become the focus of this challenge of producing metallic hydrogen, namely a path along the melting line. It has been predicted that the hydrogen melt line will have a peak and with increasing pressure the melt line may descend to zero Kelvin so that high pressure metallic hydrogen may be a quantum liquid. Even at lower pressures hydrogen may melt from a molecular solid to an atomic liquid. Earlier attempts to observe the peak in the melting line were thwarted by diffusion of hydrogen into the pressure cell components and other problems. In the second part of this paper we present a detailed description of our recent successful demonstration of a peak in the melting line of hydrogen.

PACS: **62.50.–p** High-pressure effects in solids and liquids;
64.60.Ej Studies/theory of phase transitions of specific substances;
67.63.–r Hydrogen and isotopes.

Keywords: metallic atomic phase, high pressure, melting line of hydrogen.

1. Introduction

One of the great challenges of condensed matter physics is the experimental production of metallic hydrogen in the laboratory. In 1935 Wigner and Huntington [1] predicted that at a pressure of 25 GPa (100 GPa = 1 Mbar) solid molecular hydrogen would dissociate into an atomic metallic solid. Modern measurements have extended pressures by over an order of magnitude higher than the original prediction and find that hydrogen remains in a non-metallic phase. There is little doubt that at sufficiently high density it will become a metal. The prediction of metallization at 25 GPa was early in the development of quantum mechanics in condensed matter. Modern calculations now predict much higher pressures for the insulator-to-metal (IM) transition, but still remain challenged in accuracy due to the large zero-point energy which is important at both low and high pressures and is not included as a first principles part of many approaches such as modern density functional theory.

In 1968 Ashcroft [2] predicted that atomic metallic hydrogen may be a high-T_c (possibly room temperature) superconductor, based on a BCS model. Although there were early efforts to produce metallic hydrogen with large presses, little progress was made until the late 1980s when the development of the diamond anvil cell (DAC) eventually enabled megabar pressures. In 1975 Ramaker *et al.* [3] predicted that molecular hydrogen might become metallic before dissociating, and much later Richardson and Ashcroft [4] predicted that this molecular metal might be a very high temperature superconductor, based on a non-conventional superconductivity model. Recently, Cudazzo *et al.* [5] have carried out a first principles calculation of the electron–phonon interaction and report high-T_c based on a BCS theory. They find very high T_c's, increasing with pressure, above about 450 GPa.

Early on, a number of theoretical groups became intensely interested in the high-density properties of hydrogen. Brovman *et al.* [6] predicted that when the pressure on atomic metallic hydrogen was released the atomic phase might be stabilized against the molecular phase by a 1 eV potential barrier, similar to the metastability of diamond relative to graphite. They found that metastable atomic hydrogen could even be a liquid, based on the large zero-point motion and weak interaction potentials. McDonald and Burgess [7] found that dense atomic hydrogen might not have a crystalline state. The question of

metastability at ambient pressure was considered by Salpeter [8] and remains an open question. At the present time a large number of modern calculations, reviewed elsewhere [9], have predictions that the transition to the metallic atomic phase might occur at multi-megabar pressures. Modern theoretical techniques have been extremely successful in predicting the properties of heavier more strongly interacting atomic and molecular solids as a function of density. However, hydrogen is very light and the intermolecular interactions are weak, resulting in large zero-point motion and energy. Interestingly, there is zero-point motion for the molecular centers and a zero-point motion hidden in the internal vibration of the molecule. As pressure is increased the large zero-point motion of the molecular centers decreases, but at higher pressures the internal zero-point energy of the internal motion is «liberated» to the lattice as electronic densities redistribute and modify the many-body effective intermolecular interactions, so that zero-point energy remains important. Density functional techniques cannot handle this motion and energy and do not predict correct gaps. Molecular dynamics is generally useful for classical motions, but not for hydrogen at low temperatures. Quantum Monte Carlo can handle the quantum aspects, but does not predict gaps [10].

The extension of the predicted transition pressure to higher pressures than that of Wigner and Huntington has been strongly influenced by experimental observations. Städele and Martin [11] used a modified density functional approach with exact exchange calculations to predict accurate gaps, resulting in stability of insulating molecular hydrogen against the metallic phase to 400 GPa or greater. Experimentally, Narayana *et al.* [12] reported that hydrogen remains molecular and transparent to 342 GPa, while Loubeyre *et al.* [13] reported that hydrogen turns opaque in the visible by a pressure of 320 GPa (but non-metallic) due to a closing energy gap. An explanation for this apparent contradiction will be given in the next section [14].

2. Historical developments

2.1. The metal–insulator transition

We start by discussing the highest pressure results just mentioned, that a lower pressure sample turns black while a higher-pressure sample remains transparent. Silvera [14] proposed that these seemingly contradictory reports may be explained by problems with the high-pressure ruby scale. Narayana *et al.* used the x-ray EOS of tungsten to determine the pressure, while Loubeyre *et al.* used an extrapolation of the ruby scale, which was only calibrated to 80 GPa by Mao, Xu, and Bell [15].

One of the problems of the venerable so-called quasi-hydrostatic 80 GPa calibration was that the pressurization medium, argon, is not quasi-hydrostatic at high pressure; only helium and hydrogen remain relatively soft at high pressure. Thus, to obtain an improved calibration helium should be used as the pressurization medium. A new scale based on calibration of ruby in helium, extending to 150 GPa and latest equations-of-state of metals used for the reference pressure was developed by Chijioke *et al.* [16,17]; this scale differed substantially from the earlier scale at the highest pressures of the calibration. To the extent that this scale can be extrapolated to the 300 GPa region, the pressure of Loubeyre *et al.* would be as much as 50–60 GPa higher [14], removing the contradiction.

It is now believed that hydrogen will become atomic in the 400–600 GPa region. The darkening of hydrogen and extrapolations by Loubeyre *et al.* [13], as well as later work by Baer *et al.* [18], along with a number of calculations tend to support such a belief. In Fig. 1 we show a possible phase diagram for hydrogen. There are three experimentally studied regions at lower pressures: the lowest pressure phase which has an HCP structure, the BSP, and the *A*-phases (to be discussed ahead); the high-temperature reverberating shock wave experiments of Weir *et al.* [19], who found a conducting liquid phase believed to be metallic and atomic; and the melting line to about 800 K by Datchi *et al.* [20] and Gregoryanz *et al.* [21].

An understanding of the melting line may be key to understanding the very high pressure properties of hydrogen and much of this paper will be focused on recent developments. Diatschenko *et al.* [22] first studied the melting line to 373 K and 7.7 GPa and could fit their results to a modified Simon equation. Datchi *et al.* and Gregoryanz *et al.* found that the experimental melting lines were better fit with a theoretical Kechin melting curve [23], rather than a traditional Simon curve. The Kechin form has a peak in the melting line. Scandolo [24] calculated, using density functional theory, that at high pressure the melt-

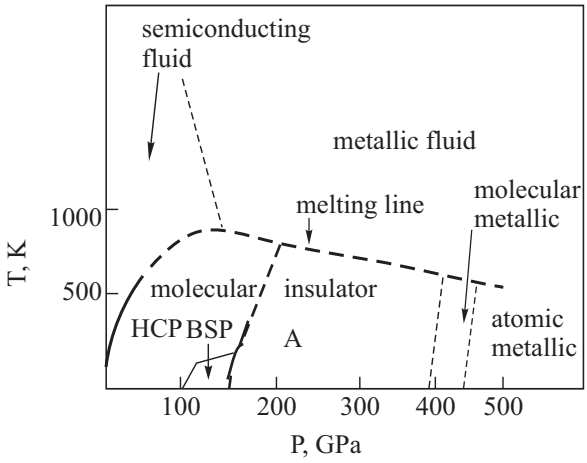

Fig. 1. Phase diagram of hydrogen including known low pressure phases (solid lines) in the insulating solid (HCP, BSP, and *A*) and possible metallic phase lines.

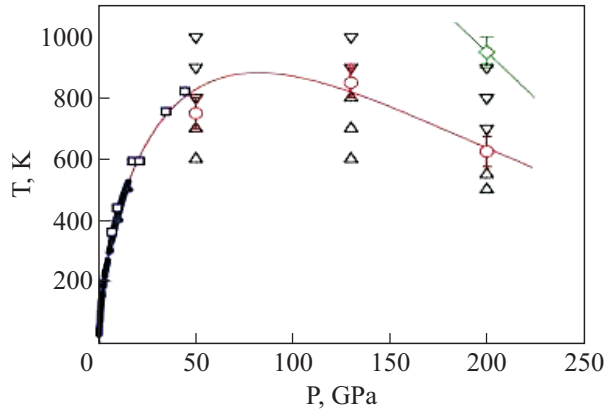

Fig. 2. The melting line of hydrogen predicted by Bonev *et al.* showing experimental data at lower pressures and temperatures. The line at high pressure and temperature with the diamond symbol is the predicted first order liquid–liquid phase transition from molecular to atomic hydrogen.

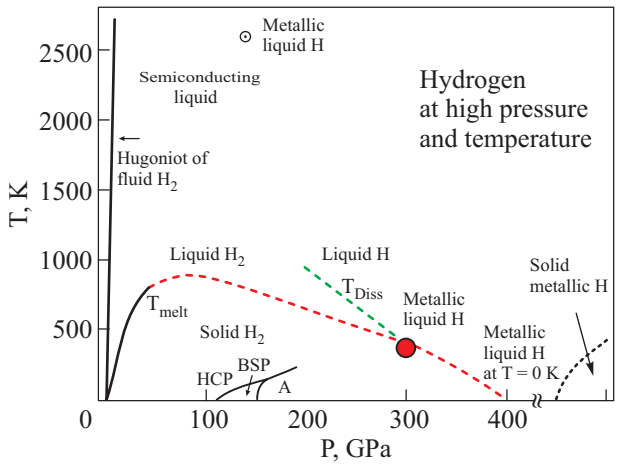

Fig. 3. Phase diagram of hydrogen at high pressure showing extrapolation of the melting line (below 700 K) to very high pressure. The melting line of Bonev *et al.* was carried out to 700 K. The recent work of Attaccalite and Sorella (filled circle) confirms the extrapolation to 400 K.

ing curve might have a negative slope. This was followed by an extensive *ab initio* molecular dynamics two-phase (liquid–solid) high-temperature melting line calculation by Bonev *et al.* [25], shown in Fig. 2. A number of remarkable results were found: the theoretical melting line indeed has a peak; the peak is below 1000 K; and in the region above the melting line there is a dissociative transition from diatomic to monatomic hydrogen (diamond marker line). Bonev *et al.*, using density functional theory found this line to be a first order phase transitions whereas Delaney *et al.* [26] using quantum Monte Carlo techniques find a continuous degree of dissociation in fluid hydrogen with increasing density. Thus, the nature of dissociation of hydrogen at high pressure and temperature is an important experimental challenge.

In a quantum solid such as helium, as pressure (density) is increased the particles at lattice sites become more localized and behave more classically. This is because with compression the effective mean field potential that a lattice particle sits in stiffens up and becomes more harmonic. In hydrogen at very high pressure it is believed that the unusual behavior of becoming more quantum (the ratio of zero-point energy to intermolecular interaction energy increases at high pressures) is due to a softening of the effective pair potentials with increasing compression. Not only are the molecules more weakly bound, but also the atom–atom bonding weakens [27]. This is supported by earlier calculations of the interactions in dense hydrogen as a function of density [28,29]. The behavior of the melting line in the region of calculation leads to some intriguing extrapolations (not yet confirmed by theory). First, (Fig. 2) the «diamond» line will intersect the melting line, so that for higher pressures solid molecular hydrogen would melt to atomic hydrogen. Second, the melting line extrapolates down to $T = 0$ K, implying that hydrogen might be an atomic metallic liquid at very high pressure. A phase diagram based on these extrapolations is shown in Fig. 3. The calculation of the melting line by Bonev *et al.*, valid for higher temperatures, did not include zero-point energy contributions so that the melting line calculations could not easily be extended to lower temperatures. More recently Attaccalite and Sorella [30] have introduced a novel *ab initio* MD calculation in which the approximation maintains validity at lower temperatures. Their work supports the extrapolation. This implies that there could be a pressure window where the metallic hydrogen is liquid at $T = 0$ K. At still higher pressures the atoms would localize into a solid.

The achievement of accurate theoretical predictions of the properties of hydrogen under pressure with regard to metallization has in general been very challenging. Thus, the first important test for this new pathway to metallic hydrogen is to demonstrate that a peak exists in the melting curve. A peak has recently been experimentally demonstrated by Deemyad and Silvera [31] and will be discussed in detail further in this paper.

The possibility of producing a (high-pressure) liquid at $T = 0$ K, with mobile electrons and protons has led to tantalizing predictions of two component superconductivity (electrons and protons) as well as superfluidity in liquid metallic hydrogen [32]. Recently, it has been shown that the Onsager–Feynman quantization as well as the London Law in a magnetic field would be violated [33]. However, we emphasize that violation of Onsager–Feynman quantization and the London law is for multi-component superconductors.

The above predictions follow from some of the most sophisticated analyzes yet. But, although the electrons were treated quantum mechanically, nuclei were classically propagated in the molecular dynamics. Furthermore, the melting line depends on the structure of the solid below the line. This has not been investigated and could have some surprises [18]. Still another possibility is that metallic hydrogen may be metastable so that once produced at high pressure it could be quenched to ambient pressure and remain in the metallic state. An experimental production of metallic hydrogen is needed to resolve these issues.

2.2. High pressure molecular phases

There are a number of high-pressure phases in the solid hydrogens. However, it is important to first consider the *ortho–para* states of the molecules, as the phase diagrams depend critically on the *ortho–para* concentrations. The instantaneous intermolecular interaction between H_2 molecules is anisotropic; however, in the solid the effective interaction depends on the rotational states of the molecules. The rotational states are labelled by the rotational quantum number J and its projection M. In the low-pressure solids, J is a good quantum number; the splitting between single-molecule rotational states is $BJ(J+1)$ where B is the rotational constant (~ 59 cm^{-1} $\approx$ ≈ 88 K, for hydrogen), whereas the anisotropic interactions are a few degrees Kelvin. Since the rotational splittings are hundreds of degrees at low temperature, in equilibrium the $J=0$ state is the single-molecule ground state. The wave function for $J=0$, the spherical harmonic $Y_{JM}(\theta,\phi)=Y_{00}$, is a constant so that the molecules are in spherically symmetric states. As a result, for *para* hydrogen the expectation value for the anisotropic intermolecular interactions is zero when the interactions are evaluated for the quantum states. The many-body ground state of the solid is close-packed (HCP), like rare gas solids. As pressure is increased, the instantaneous (non-quantum expectation value) anisotropic interactions grow so that the spherical harmonics become a poorer description of the single-molecule states. At a critical pressure, the admixture of J states becomes so large that J is no longer a good quantum number and the ground molecular states become non-spherical. This breaks the symmetry of the ground state as a quantum phase transition and the molecules go into an orientationally ordered phase called the broken symmetry phase (BSP). By contrast, solid $J=1$ molecules have p-like distributions and the solids are orientationally ordered in the $Pa3$ structure at zero-pressure and low temperature [34]. Thus, the ground state of the solid depends on the *ortho–para* species. One of the most important points is that for the homo-nuclear diatomic hydrogens, isolated *ortho*- and *para* molecules do not thermalize with each other and behave as non-identical molecules.

The *ortho–para* states are a result of the Pauli Principle. Consider isolated hydrogen molecules: the wave function must be antisymmetric under proton exchange. Thus, the symmetric even-J rotational states are coupled to the antisymmetric nuclear spin singlets, with $I=0$, and the odd-J states are coupled to the triplet $I=1$ states. The former are called *para*-hydrogen and the latter *ortho*-hydrogen. The nomenclature changes for deuterium (in which the deuterons are spin−1 bosons and the molecular wavefunctions are symmetric under nucleon exchange). The ground state with $J=0$ is *ortho*-deuterium (even-J combines with symmetric $I=0,2$ nuclear states) and the odd-rotational states combine with $I=1$ spin states. Thus, *para*-hydrogen and *ortho*-deuterium behave similarly. A key point is that transitions between *ortho* and *para* (conversion) are strongly forbidden for isolated molecules, and the conversion rate is very slow in the interacting low-pressure solid state. A zero-pressure solid can take from days to weeks to come to the thermal equilibrium for the occupation of the rotational states. Thus, it is possible to produce and study almost pure *ortho*-hydrogen or *para*-deuterium [35] that is out-of-equilibrium and metastable. As pressure is increased, the *ortho–para* description remains valid, even though the single-molecule states change. This was not always clear throughout the community and it was thought that under pressure this description was not valid [36]. This picture was clarified theoretically by Silvera [37].

It is most interesting to study solids of the pure species, and methods exist for producing high purity *ortho* or *para* samples. It is clearly vital to know the *ortho–para* concentration of a sample. In general, this is difficult to measure in a DAC, but if the initial concentration and the conversion rate are known, then one can determine the state of the solid as a function of time. At elevated pressures the conversion rates increase [38,39] so that conversion to equilibrium may take hours rather than weeks. Hydrogen converts much faster than deuterium, as the conversion mechanism depends principally on the nuclear magnetic moment, which is much larger in hydrogen.

In a DAC at high pressure and low temperature (less than ~ 20 K) a pure *ortho*-hydrogen sample will down convert to *para*-hydrogen, whereas a *para*-hydrogen sample is stable. Thus, it is much easier to study the $J=0$ species, maintaining the system at low temperature, with short time excursions to higher temperatures. It is also more interesting because of the BSP quantum phase transition. Most studies have been on *para*-hydrogen or *ortho*-deuterium, and of course *ortho–para* mixtures, unfortunately usually with an undetermined concentration.

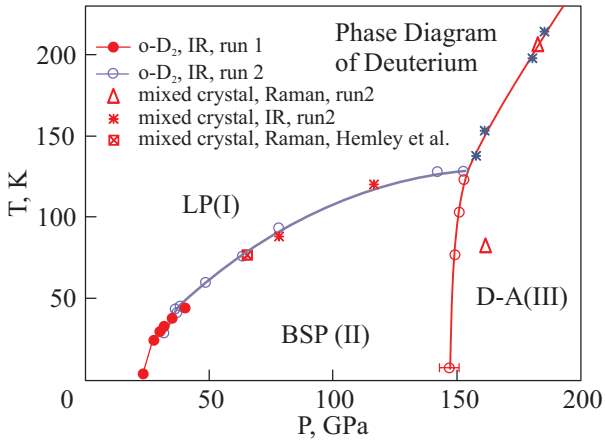

Fig. 4. The high pressure phase diagram of *ortho*-deuterium showing the LP, BSP and *A*-phases.

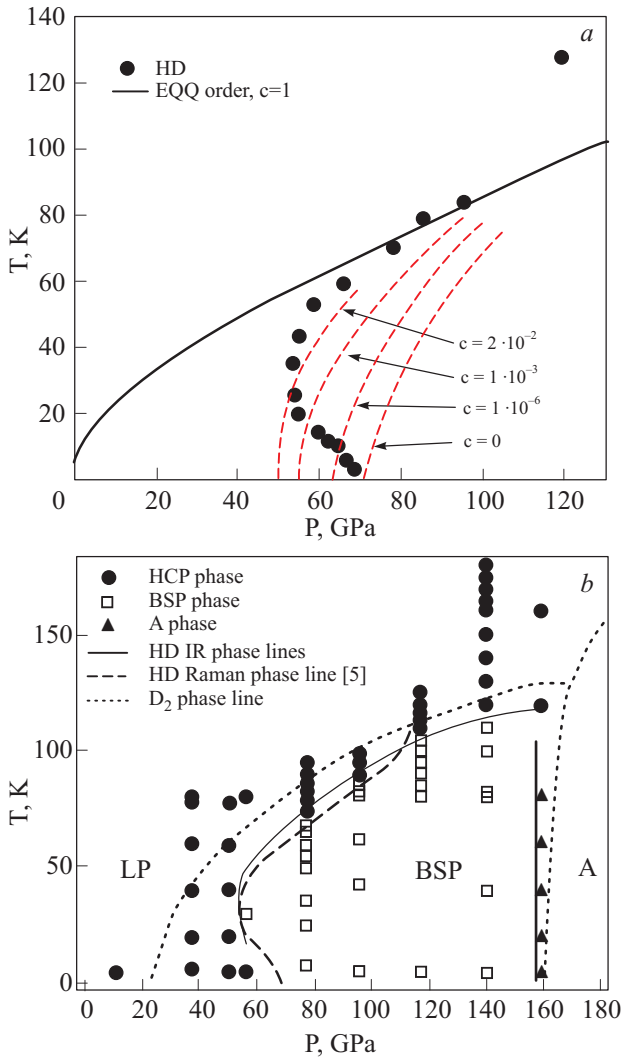

Fig. 5. The phase diagram of HD: as determined by Raman scattering (*a*); by IR spectroscopy (*b*). The symbols represent *P–T* points where infrared spectra were recorded to determine the phase diagram.

At present there are three well-defined high-pressure phases that have been experimentally observed in the solid molecular hydrogens. An example of the phase diagram for *ortho*-deuterium [40] is shown in Fig. 4; a similar diagram exists for *para*-hydrogen. The LP phase (low pressure, sometimes called phase I) is an HCP solid; the BSP (broken symmetry phase), first predicted by Raich and Etters [41], exhibits orientational order of *para*-hydrogen and has been observed in D_2, H_2, and HD (at 28, 110, and 69 GPa, respectively, in the $T = 0$ limit [42–44]). At higher pressures a transition to a new phase called the *A*-phase (III) takes place. This phase was unexpected and is believed to be a transition to a lower energy phase of orientational order [45]. The *A*-phase occurs at around 150 GPa for hydrogen and deuterium [46,47]. This phase was first reported to be metallic [48,49], but later it was shown that it is molecular insulator [50–53]. No other phases have yet been found at higher pressures in the solid.

This background introduction is completed with a discussion of hydrogen deuteride. HD turns out to be a very interesting, unusual solid for high-pressure studies. It does not have the *ortho–para* designation, as the two nuclei in a molecule are not identical. As a consequence, the transitions between even and odd J states are rapid and the molecular states in the solid thermalize within milliseconds. This has a dramatic effect on the BSP phase line which is reentrant, as seen in Fig. 5 [44,54], compared to the monotonically increasing phase line of hydrogen or deuterium. Silvera *et al.* [55] explained this by the thermal population of the $J = 1$ state. They proposed that for each fixed concentration of $J = 1$ there is a different phase line, as shown by the dashed lines in Fig. 5,*a*. As temperature is increased in HD and the $J = 1$ states become occupied, the phase line traverses from each of these fictitious lines to another; as temperature is increased further, the BSP phase disorders for entropic reasons, leading to the reentrant behavior. Recently, Hetenyi *et al.* [56] have developed a molecular field model for quantum rotors which reproduces most of the features of orientational ordering.

In the experimental work the phase line was determined by a shift in the Raman active vibron mode as the phase line was crossed, as was done in hydrogen and deuterium. However, in HD the shift goes through zero at about 100 GPa (the shift does not change sign in the homonuclear species); the Raman lines rapidly broaden so that it is difficult to follow the phase line to higher pressures and the uncertainties become large. Recently, Chijioke and Silvera [54] have extended the phase diagram of HD to higher pressures, and determined the onset of the *A*-phase (Fig. 5,*b*). They used infrared absorption, as there are IR active vibrons in the BSP phase and none in the LP phase, so the BSP–LP phase line could be ex-

tended to higher pressures. The emergence of the *A*-phase was detected by observation of a new IR active vibron.

HD has one more feature that distinguishes it from the homonuclear diatomic hydrogens, and that is a permanent electric dipole moment, resulting from the displacement of the electronic charge from the nuclear charge. With a permanent dipole moment, **p**, the rotational transitions are IR active, which enabled Trefler and Gush [57] to spectroscopically determine its value to be $5.85 \cdot 10^{-4}$ D.

3. The melting line of hydrogen

Over the past decades the pathway to metallic hydrogen that has been followed has been to compress solid hydrogen at low temperature to a sufficiently high density to achieve metallization. In recent years the possibility of a high temperature pathway along the melting line has opened up. Although multi-megabar pressures can be achieved in DACs, the temperature range for studying the hydrogen melting line by continuous heating to elevated temperatures has been limited by diffusion of hydrogen into the gasket or diamonds, followed by embrittlement and failure of the diamonds. Datchi *et al.* [20] extended the range of the melting line to 526 K and 15 GPa. This experiment was limited in temperature as hydrogen diffused into the metallic gasket at high temperature and the sample was lost. Gregoryanz *et al.* [21] extended these measurements to around 800 K and 44 GPa using a ceramic insert in their gasket that confined the hydrogen long enough for measurements. Their extension of the melting line terminated when they could no longer distinguish melting by a shift in the Raman active vibron when crossing the melting line. At elevated temperatures the diamonds would embrittle due to hydrogen diffusion and fail [58]. Both groups found a better fit of the melting line to a Kechin curve that implied a peak in the melting line at higher pressures.

Diffusion is a relatively slow and thermally activated process; hydrogen does not significantly diffuse into diamond at low temperature. In order to study the melting line at higher temperatures the diffusion must be slowed or inhibited. There are two conventional ways by which samples are heated in diamond anvil cells: resistive heating, as was done by Datchi *et al.* [20] and Gregoryanz *et al.* [21], and CW laser heating [59,60]. In the latter technique, a high power laser beam is focused on an absorber in a DAC, as shown in Fig. 6. Laser power as high as 50 W is used to achieve temperatures of thousands of degrees. The diamonds also heat but insulation between the hot sample absorber and the diamond surface prevents the diamond from burning or graphitizing. Both of these methods allow diffusion of hydrogen or helium into the diamond and seriously limit the time that a sample of hydrogen can be studied at high temperatures.

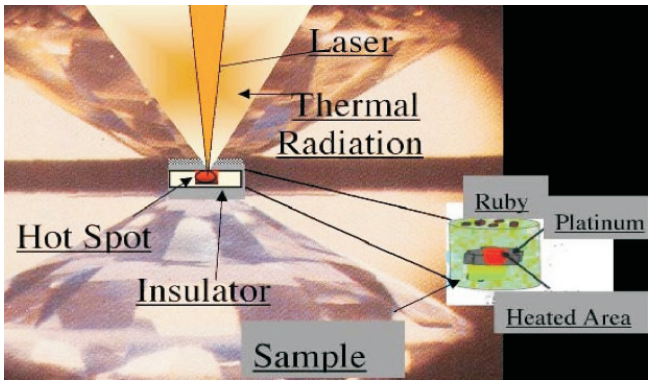

Fig. 6. Laser heating in the heart of a DAC showing a sample in a gasket between two diamonds. The laser power heats a «black» absorber (platinum) embedded in a sample along with a grain of ruby for pressure determination. Temperature is determined by collecting the thermal black-body radiation in a spectrometer and fitting to the Planck function. Diamonds must be insulated from the hot sample to prevent excessive heating and burning.

To overcome this problem we have used the method of pulsed laser heating to heat samples in DACs [61] and developed a method to determine the peak temperature of the sample using CW detection. In this method a platinum foil is embedded in the hydrogen sample acting as a laser absorber; it is the foil that heats and warms the adjacent hydrogen pressing on its surface. Two advantages exist for pulsed laser heating of hydrogen to reduce hydrogen diffusion into the confining elements. First, hydrogen mainly diffuses during the hot pulse and this time is insufficient for important diffusive changes. Second, the gasket and diamonds do not get very hot [62]. The latter can be justified by the following argument. Although energy is flowing from the absorber to the hydrogen to the diamonds, the thermal time constants of the components and sample are very different. The metallic absorber is substantially smaller than the hydrogen sample and has a short thermal time constant compared to that of the hydrogen. The surface of the absorber warms during the pulse; the energy then diffuses into the absorber in several microseconds to a much lower temperature than the peak temperature. The excess thermal energy from the absorber flows into the hydrogen at an even lower temperature and is conducted away into the high thermal conductivity diamonds until the DAC reaches ambient temperature.

We use a Spectra Physics pulsed neodymium vanadate laser operating at 1.064 μm. A pulse of width $\tau \sim 70$ to 200 ns with an energy of a few milijoules (pulse power can be up to of order ~30 kW) is more than sufficient to heat the sample so that it is in local thermal equilibrium (a few ps is sufficient for thermalization). The sample heats and cools (in several laser pulse widths). With a low pulse repetition rate, the average power of the laser is

only a few hundred miliwatts, so that the average temperature remains low.

Accurate measurement of the peak temperature during pulsed laser heating can be accomplished. Pulsed heating was first reported by Basset and Weathers [63]; however, they measured the thermal radiation emitted from the sample throughout the heating and cooling period of the sample, and when fitted to a Planck function this gives a temperature lower than the peak temperature. The blackbody radiation energy flux at wavelength λ is

$$F_\lambda = \frac{15\sigma T^4}{\pi^4}\frac{kT}{hc}\frac{x^5}{(e^x - 1)}. \qquad (1)$$

This varies as T^5; σ is the Stefan–Boltzmann constant, $x \equiv hc/\lambda kT$, and the other symbols have their usual meaning. Due to the strong temperature dependence most of the radiation is emitted at the peak temperature, T_{peak}. This irradiance *vs* wavelength can be fitted reasonably well to a blackbody curve to give an effective temperature that can be a few hundred K lower than the peak temperature, depending on the magnitude of Tpeak. The correction can be calculated by convolving the blackbody curve with the heating curve,

$$\bar{F}_\lambda = \int_0^\infty F_\lambda\,[T(t)]\,dt\,, \qquad (2)$$

which is determined using the measured laser pulse shape and the material properties. A correction table can be developed and the peak temperature can be determined [61].

Conventionally one measures the blackbody irradiance as a function of wavelength in the visible with a spectrometer and an integrating CCD photo detector. This technique yields high precision for temperatures above ~1000 K. This procedure can be used for accurate measurements in a DAC but the irradiance falls off rapidly with decreasing temperature as shown in Fig. 7, and the peak irradiance shifts into the infrared. Since the predicted temperatures for the melt line were below 1000 K we developed an optical pyrometer for use in the IR using narrow band IR filters [65] and a cooled InSb detector, shown in Fig. 8.

A diamond anvil cell capable of achieving pressures in the megabar range was cryogenically loaded with hydrogen. The cell was removed from the cryostat so that the ambient temperature of the pressurized hydrogen was room temperature. The absorber was a platinum foil sitting on ruby chips to separate it from the diamond surface by a layer of hydrogen so that the diamonds would not be in direct contact with the heated absorber. The ruby chips also served to measure the pressure by the wavelength shift of the ruby fluorescence peak, using a recently improved pressure scale [16]. The solid–liquid melting temperature was measured in two ways. As shown in Fig. 8, we use a video monitor to observe the absorber surface when it is heated. The monitoring CCD camera responds to the pulsed laser wavelength, so that we observe the surface only when it is heated (the pulse repetition rate was 20 KHz). We monitor the laser speckle and this speckle pattern starts to move when the hydrogen melts. The second method is to plot the temperature *vs* average laser power, shown in Fig. 9. In the Fig. 9,*a* we show plateaus used to determine the melting temperature; these plateaus were found to agree with the visual observation of the melting. Plateaus at the melting line are ubiquitous, and there are various explanations in the literature. When the laser power is increased and hydrogen melts, the incremental pulsed laser power goes into the heat of melting

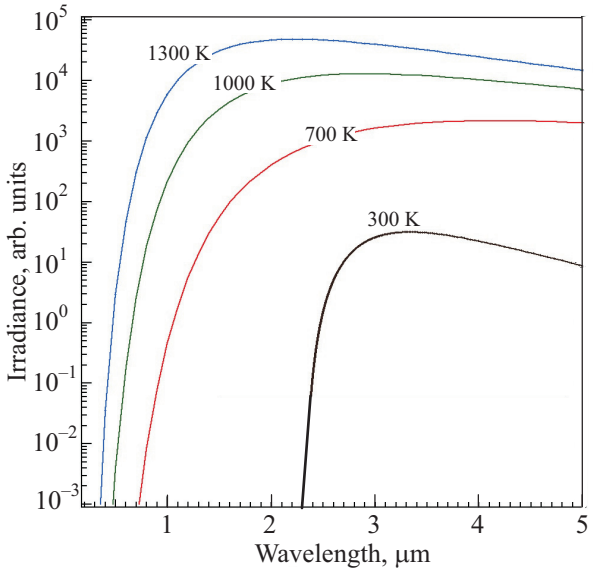

Fig. 7. Calculated black-body irradiance on an logarithmic scale as a function of wavelength for several temperatures shown in the legend.

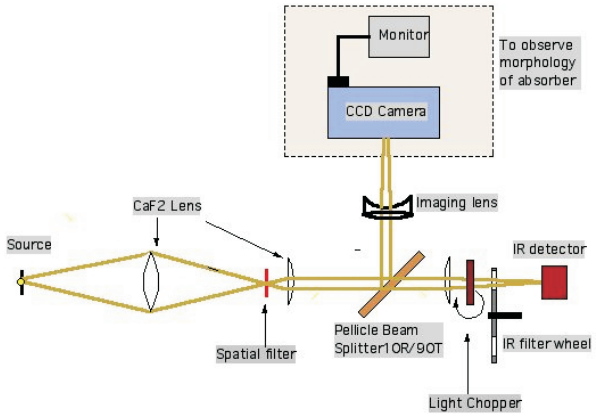

Fig. 8. The optical layout used for measuring the spectral irradiance in the infrared and for visually monitoring the melting of the hydrogen.

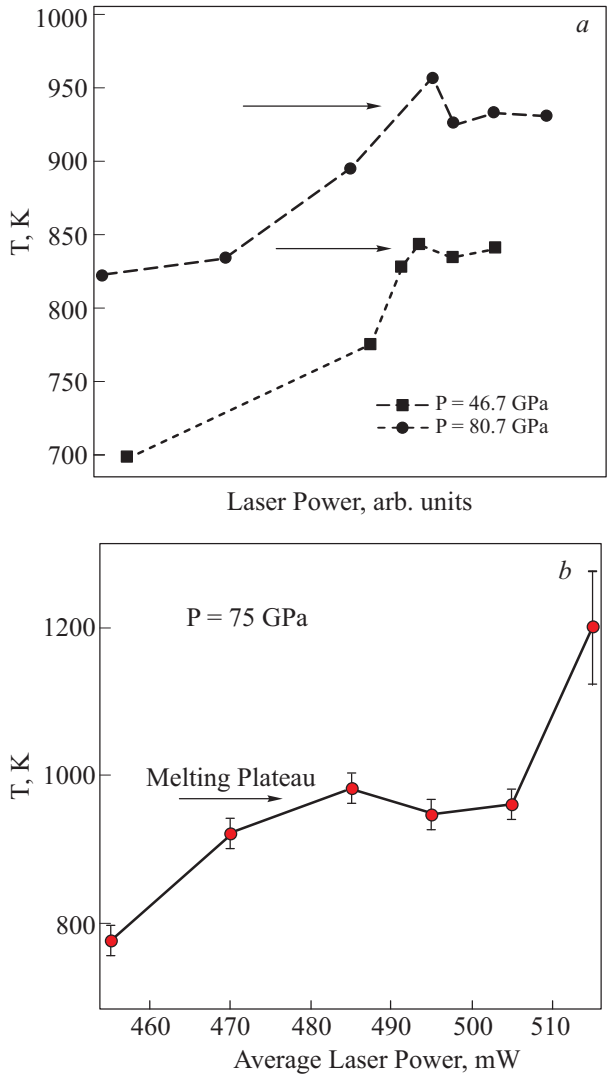

Fig. 9. Plots of the peak temperature *vs* average laser power showing the rise in temperature and the plateaus when the hydrogen melts, for two different pressures (*a*). A plot of the plateau at 75 GPa showing the rise in temperature beyond the plateau. The temperature was determined with 5 narrow band filters (*b*). In this case a single filter was used, resulting in larger uncertainties in the temperature.

and as the power is increased the pool of melted hydrogen increases, resulting in the plateau, without the rise in temperature found in the single-phase solid. The heat of the melted region flows into the solid region. Eventually, the power input to the melt is faster than the heat can be carried away and the temperature of the melt (and absorber) again rises. This is shown in the Fig. 9,*b*. As this was the our first high-temperature melting line measurement with hydrogen, for most of the pressure points we were conservative in going to very high temperature to avoid possible increased diffusion, so in most runs we did not demonstrate the temperature rise beyond the plateau.

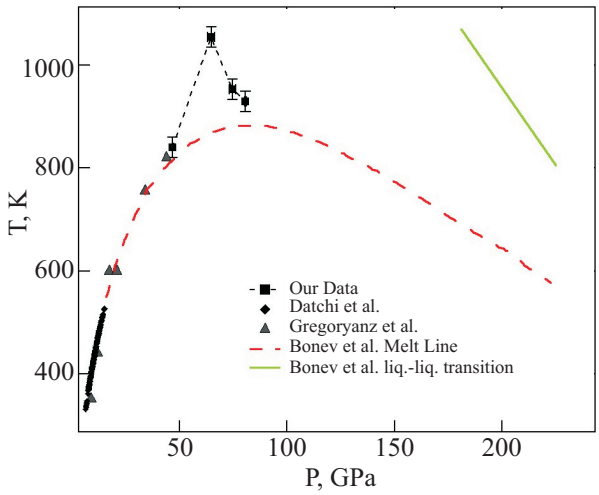

Fig. 10. The experimental melting line of hydrogen showing our results along with earlier results at lower pressures. The dashed curve is fit to the theoretical result of Bonev *et al.* fit to a Kechin curve. The solid line is the calculated liquid–liquid phase line for dissociation of hydrogen in the melt.

Our experimental extension of the melting line is shown in Fig. 10 and has a peak. Our lowest pressure point overlaps the data of Gregoryanz *et al.* who measured the temperature with a thermocouple. The data exhibits a rather sharp peak at (64.7 ± 4) GPa and (1055 ± 20) K, and the data set cannot be fit with a Kechin curve. The pressure was measured before and after heating. The pressure during the pulsed heating might be enhanced by 5–10% due to a thermal effect demonstrated by a finite element analysis. The unexpectedly sharp structure of the melting line may imply some unanticipated behavior in the solid or the liquid.

This first observation of a peak and the extension of the melting line to higher pressures was terminated for an unusual reason. Generally high-pressure experiments extending into the megabar pressure region are ended by failure of the diamond anvils. In our case, as pressure was increased, the signal from the ruby chips utilized to measure the pressure became weaker. The ruby signal was observed before and after heating cycles, and the second measurement was always weaker. Eventually, as the pressure approached 100 GPa we could no longer excite the ruby fluorescence, and other techniques of measuring the pressure were not successful [31]. Since we had observed the long sought after peak in the melting line, we ended the experiment. We suspected that the ruby fluorescence might have been quenched by hydrogen diffusion into the ruby chips which were embedded in the hydrogen and heated during the laser pulsing as they were in contact with the absorber. A few hours after ending the experiment we started measuring the ruby signal from one of the chips as a function of time. In Fig. 11 we show the integrated intensity of the ruby fluorescence line as a function

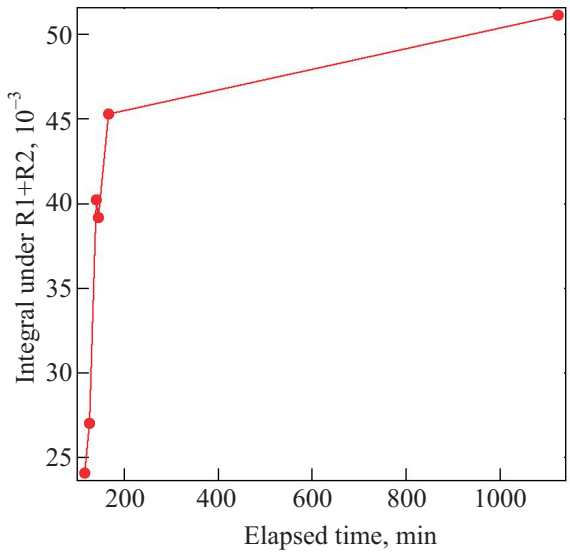

Fig. 11. Recovery of ruby signal as a function of time after experiment was terminated and ruby chips were at room temperature and pressure in air.

of time showing the recovery of the signal due, we assume, to the out-diffusion of hydrogen. Overnight, the ruby recovered its full signal, shown by the point at longest time. The frequency of the ruby R1 peak did not measurably shift with time. Thus, we assume the same was true under pressure, so that the ruby pressure scale could be used with some confidence for determining the sample pressure. In the future this problem can be easily overcome by exciting ruby chips that are not in contact with the absorber and heated.

The technique of pulsed laser heating of hydrogen at high pressure has been demonstrated to overcome the problems that limited earlier researchers from extending the melting line to higher pressures and temperatures. It is our intention to extend the melting line to higher pressures in the megabar range by this new method. It may be a new pathway to metallic hydrogen.

1. E. Wigner and H.B. Huntington, *J. Chem. Phys.* **3**, 764 (1935).
2. N.W. Ashcroft, *Phys. Rev. Lett.* **21**, 1748 (1968).
3. D.E. Ramaker, L. Kumar, and F.E. Harris, *Phys. Rev. Lett.* **34**, 812 (1975).
4. C.F. Richardson and N.W. Ashcroft, *Phys. Rev. Lett.* **78**, 118 (1997).
5. P. Cudazzo, G. Profeta, A. Sanna, A. Floris, A. Continenza, S. Massidda, and E.K.U. Gross, *Phys. Rev. Lett.* **100**, 257001 (2008).
6. E.G. Brovman, Y. Kagan, and A. Kholas, *Sov. Phys. JETP* **34**, 1300 (1972).
7. A.H. MacDonald and C.P. Burgess, *Phys. Rev.* **B26**, 2849 (1982).
8. B.B. Salpeter, *Phys. Rev. Lett.* **28**, 560 (1972).
9. I.F. Silvera, in: *Metal–Insulator Transitions Revisited*, P.P. Edwards and C.N.R. Rao (eds.), Taylor & Francis, London (1995), p. 21.
10. V. Natoli, R.M. Martin, and D.M. Ceperley, *Phys. Rev. Lett.* **70**, 1952 (1993).
11. M. Städele and R.M. Martin, *Phys. Rev. Lett.* **84**, 6070 (2000).
12. C. Narayana, H. Luo, J. Orloff, and A.L. Ruoff, *Nature* **393**, 46 (1998).
13. P. Loubeyre, F. Occelli, and R. Le Toullec, *Nature* **416**, 613 (2002).
14. I.F. Silvera, in: *AIRAPT, Forschungszentrum Karlsruhe, Germany*, http://bibliothek.fzk.de/zb/verlagspublikationen/AIRAPTEHPRG2005/, Karlsruhe (2005).
15. H.K. Mao, J. Xu, and P.M. Bell, *J. Geophys. Res.* **91**, 4673 (1986).
16. A.D. Chijioke, W.J. Nellis, A. Soldatov, and I.F. Silvera, *J. Appl. Phys.* **98**, 114905 (2005).
17. A.D. Chijioke, W.J. Nellis, and I.F. Silvera, in: *Shock Compression of Condensed Matter, 2005*, M.E.E.M D. Furnish, T.P. Russell, and C.T. White (eds.), AIP Press, Baltimore (2005).
18. B.J. Baer, W.J. Evans, and C.-S. Yoo, *Phys. Rev. Lett.* **98**, 235503 (2007).
19. S.T. Weir, A.C. Mitchell, and W.J. Nellis, *Phys. Rev. Lett.* **76**, 1860 (1996).
20. F. Datchi, P. Loubeyre, and R. Le Toullec, *Phys. Rev.* **B61**, 6535 (2000).
21. E. Gregoryanz, A.F. Goncharov, K. Matsuishi, H.K. Mao, and R. J. Hemley, *Phys. Rev. Lett.* **90**, 175701 (2003).
22. V. Diatschenko, C.W. Chu, D.H. Liebenberg, D.A. Young, M. Ross, and R.L. Mills, *Phys. Rev.* **B32**, 381 (1985).
23. V.V. Kechin, *J. Phys.: Condens. Matter* **7**, 531 (1995).
24. S. Scandolo, *Proc. Nat. Acad. Sci. (USA)* **100**, 3051 (2003).
25. S.A. Bonev, E. Schwegler, T. Ogitsu, and G.Galli, *Nature* **431**, 669 (2004).
26. K.T. Delaney, C. Pierleoni, and D.M. Ceperley, *Phys. Rev. Lett.* **97**, 235702 (2006).
27. F. Moshary, N.H. Chen, and I.F. Silvera, *Phys. Rev.* **B48**, 12613 (1993).
28. K. Nagao, S.A. Bonev, A. Bergara, and N.W. Ashcroft, *Phys. Rev. Lett.* **90**, 035501 (2003).
29. N.W. Ashcroft, *J. Phys.* **A36**, 6137 (2003).
30. C. Attaccalite and S. Sorella, *Phys. Rev. Lett.* **100**, 114501 (2008).
31. S. Deemyad and I.F. Silvera, *Phys. Rev. Lett.* **100**, 155701 (2008).
32. B. Babaev, A. Sudbo, and N.W. Ashcroft, *Nature* **431**, 666 (2004).
33. E. Babaev and N.W. Ashcroft, *Preprint* (2006).
34. W.N. Hardy, I.F. Silvera, and J.P. McTague, *Phys. Rev. Lett.* **26**, 127 (1971).
35. I.F. Silvera, *Rev. Mod. Phys.* **52**, 393 (1980).
36. H. Mao and R.J. Hemley, *Rev. Mod. Phys.* **66**, 671 (1994).
37. I.F. Silvera, *J. Low Temp. Phys.* **112**, 237 (1998).
38. J.H. Eggert, E. Karmon, R.J. Hemley, H.K. Mao, and A.F. Goncharov, *Proc. Nat. Acad. Sci. (USA)* **96**, 12269 (1998).
39. M.G. Pravica and I.F. Silvera, *Phys. Rev. Lett.* **81**, 4180 (1998).

40. L. Cui, N.H. Chen, S.J. Jeon, and I.F. Silvera, *Phys. Rev. Lett.* **72**, 3048 (1994).
41. J.C. Raich and R.D. Etters, *J. Low Temp. Phys.* **22**, 213 (1972).
42. I.F. Silvera, and R.J. Wijngaarden, *Phys. Rev. Lett.* **47**, 39 (1981).
43. H.E. Lorenzana, I.F. Silvera, and K.A. Goettel, *Phys. Rev. Lett.* **64**, 1939 (1990).
44. F. Moshary, N.H. Chen, and I.F. Silvera, *Phys. Rev. Lett.* **71**, 3814 (1993).
45. I.I. Mazin, R.J. Hemley, A.F. Goncharov, M. Hanfland, and H.K. Mao, *Phys. Rev. Lett.* **78**, 1066 (1997).
46. R.J. Hemley and H.K. Mao, *Phys. Rev. Lett.* **61**, 857 (1988).
47. H.B. Lorenzana, I.F. Silvera, and K.A. Goettel, *Phys. Rev. Lett.* **63**, 2080 (1989).
48. H.K. Mao, and R.J. Hemley, *Science* **244**, 1462 (1989).
49. H.K. Mao, R.J. Hemley, and M. Hanfland, *Phys. Rev. Lett.* **65**, 484 (1990).
50. I.F. Silvera, *J. Non-Cryst. Solids* **205–207**, 290 (1995).
51. N.H. Chen, B. Sterer, and I.F. Silvera, *Phys. Rev. Lett.* **76**, 1663 (1996).
52. M. Eremets, *private communication and reported at conferences.*
53. R.J. Hemley, H.K. Mao, A.F. Goncharov, M. Hanfland, and V. Struzhkin, *Phys. Rev. Lett.* **76**, 1667 (1996).
54. A. Chijioke and I.F. Silvera, *Phys. Rev. Lett.* **97**, 255701 (2006).
55. I.F. Silvera, in: *HEDM Conference, Woodshole, Massachusetts* (1993).
56. B. Hetenyi, S. Scandolo, and B. Tosatti, *Phys. Rev. Lett.* **94**, 125503 (2005).
57. M. Trefler and H.P. Gush, *Phys. Rev. Lett.* **20**, 703 (1968).
58. E. Gregoryanz, *private communication*.
59. W.A. Bassett, *Rev. Sci. Instr.* **72**, 1270 (2001).
60. R. Boehler, *Rev. Geophys.* **38**, 221 (2000).
61. S. Rekhi, J. Tempere, and I.F. Silvera, *Rev. Sci. Instr.* **74**, 3820 (2003).
62. J. Tempere and I.F. Silvera: *this has been shown by finite element analysis (FEA); unpublished*.
63. W.A. Bassett and M.S. Weathers, *Physica* **139 &140**, 900 (1986).
64. S. Deemyad, B. Sterer, C. Barthel, S. Rekhi, J. Tempere, and I.F. Silvera, *Rev. Sci. Instr.* **76**, 125104 (2005).
65. P. Shuker, A. Melchior, Y. Assor, D. Belker, and E. Sterer, *Rev. Sci. Instr.* **79**, 073908 (2008).